

# Dynamic Matching System for Radio-Frequency Plasma Generation

Anas Al Bastami, *Student Member, IEEE*, Alexander Jurkov, *Student Member, IEEE*, Parker Gould, Mitchell Hsing, Martin Schmidt, *Fellow, IEEE*, Jung-Ik Ha, *Senior Member, IEEE*, and David J. Perreault, *Fellow, IEEE*

**Abstract**—Plasma generation systems represent a particularly challenging load for radio-frequency power amplifiers owing to the combination of high operating frequency (e.g., 13.56 MHz) and highly variable load parameters. We introduce a dynamic matching system for Inductively Coupled Plasma (ICP) generation that losslessly maintains near-constant driving point impedance (for low reflected power) across the entire plasma operating range. This new system utilizes a Resistance Compression Network (RCN), an impedance transformation stage, and a specially-configured set of plasma drive coils to achieve rapid adjustment to plasma load variations. As compared to conventional matching techniques for plasma systems, the proposed approach has the benefit of relatively low cost and fast response, and does not require any moving components. We describe suitable coil geometries for the proposed system, and treat the design of the RCN and matching stages, including design options and tradeoffs. A prototype system is implemented and its operation is demonstrated with low pressure ICP discharges with  $O_2$ ,  $C_4F_8$ , and  $SF_6$  gases at 13.56 MHz and over the entire plasma operating range of up to 250 W.

**Index Terms**—Impedance matching, Impedance transformation, Plasma generation, Resistance compression network, Tunable matching network, Antenna tuning unit, Inductively-coupled plasma.

## I. INTRODUCTION

THE use of plasma in the processing of materials has become prevalent in a wide range of industries [1]–[3]. A commonly used means of generating these plasmas is to inductively couple energy from a radio-frequency (RF) power amplifier into the chamber containing the gas to be ionized, (e.g., by driving RF current through a coil wound around the chamber). Key challenges in RF plasma generation include efficiently generating and controlling the RF power delivered into the plasma, while maintaining acceptable loading of the associated RF power amplifier under the highly-variable conditions in a plasma system. Inductively-Coupled Plasma (ICP) loads represent a dynamically-variable load impedance that depends on gas type and pressure, operating mode, power level, and other features. For example, in processes such as the Bosch process for reactive ion etching, there is a frequent change of the gas being ionized, which can contribute to the

variation in the impedance presented by the coil [4], [5]. The effective load impedance can vary substantially in both its real and reactive components, making matching challenging.

Power amplifiers (including switched-mode amplifiers or inverters) used to generate the plasmas are typically designed to operate efficiently and deliver their rated power into a fixed load resistance (e.g., a  $50\ \Omega$  termination). Moreover, the performance of many high-frequency (HF, 3-30 MHz) switched-mode power amplifiers / inverters degrades quickly with variations in load impedance, e.g., [6]–[8]. Because the effective loading provided by the plasma coil varies greatly across operating conditions, a tunable matching network (TMN) or “Antenna Tuning Unit” (ATU) is typically utilized between the power amplifier and the plasma coil. A TMN typically comprises a matching network having adjustable passive components that are dynamically tuned, such as by using servo motors to mechanically adjust a set of variable capacitors and/or inductors, by using switched capacitor and/or inductor banks, or by using high-power varactors. Such TMN units are very effective, and can present a constant (e.g.,  $50\ \Omega$ ) input impedance across the entire range of the plasma operation [9]–[11], but tend to be costly, bulky, and exhibit a slow response to load changes. Inverters or power amplifiers that can directly drive the wide impedance range in ICP applications at HF frequencies may be possible, but are presently in only a very nascent stage of development [12].

This paper, which represents an expansion of the authors’ conference paper [13], introduces a new approach to driving inductively-coupled plasma that provides narrow-range loading of the power amplifier with lossless, high-bandwidth adjustment for plasma load variations. It also has relatively small size and cost, and doesn’t require moving or switchable components. The proposed approach comprises a set of specially-configured plasma drive coils along with an impedance matching system based on a resistance compression network [6], [14]–[16]. Section II of the paper describes the overall structure and operation of the proposed system, including the coil design and resistance compression network. Section III describes the design of a prototype system demonstrating the approach, Section IV presents experimental results, and Section V discusses the performance of two-port matching networks. Lastly, Section VI concludes the paper.

## II. SYSTEM ARCHITECTURE

Figure 1 illustrates the proposed plasma drive and matching system, while Figure 2 shows a conceptual illustration of

A. Al Bastami, A. Jurkov, P. Gould, M. Hsing, M. Schmidt, and D. Perreault are with the Department of Electrical Engineering and Computer Science, Massachusetts Institute of Technology, Cambridge, MA, 02139 USA (e-mails: abastami@mit.edu; asjurkov@mit.edu; pgould@mit.edu; mhsing@mit.edu; djperrea@mit.edu).

J. Ha is with the Department of Electrical Engineering and Computer Science, Seoul National University, Seoul 151-744, Korea (e-mail: jungikha@snu.ac.kr).

Manuscript received February XX, 2017; revised XXXX XX, 2017.

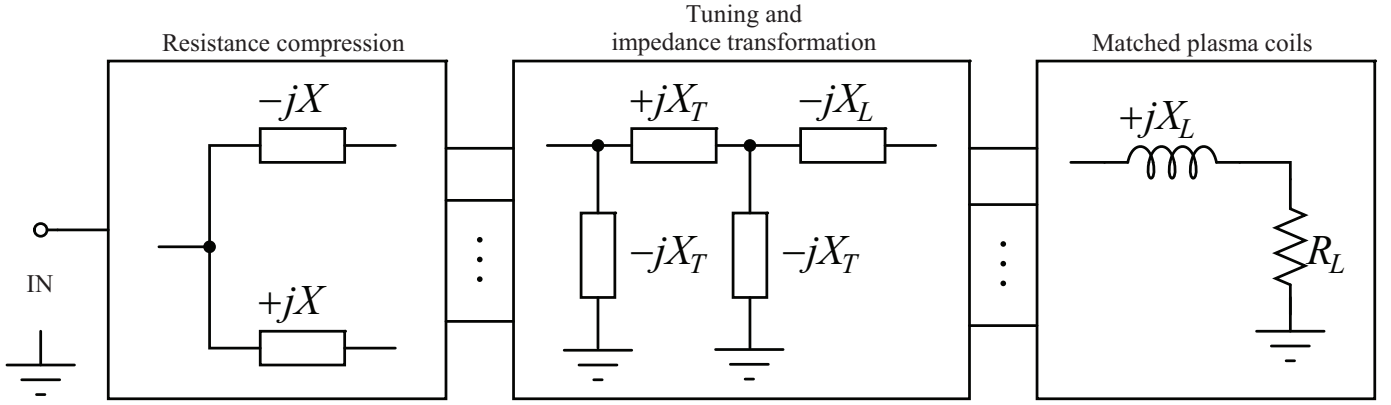


Fig. 1. Structure of the overall matching system. Each plasma drive coil is modeled as a reactance in series with a resistance.

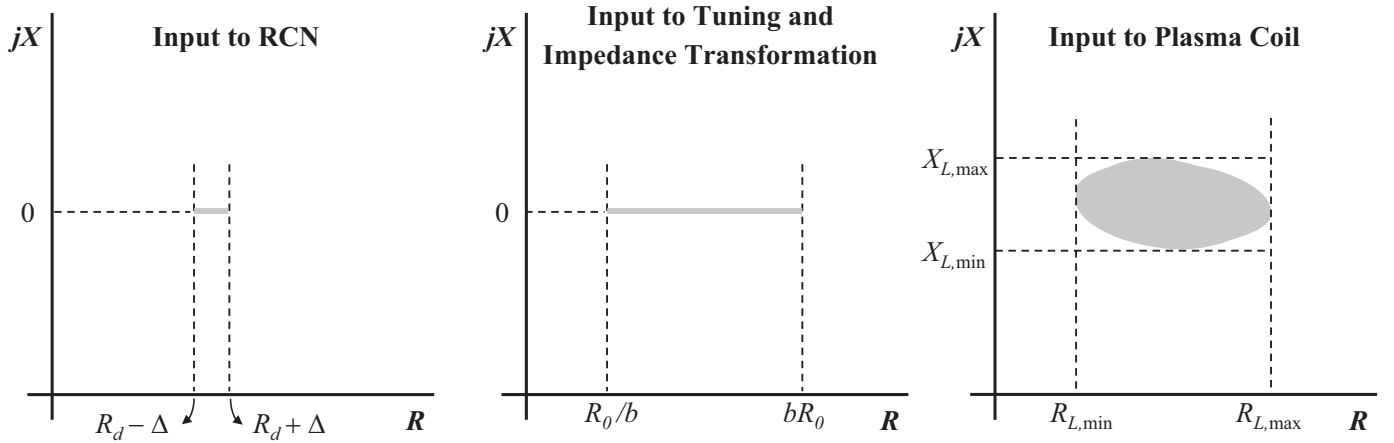


Fig. 2. Conceptual illustration of the effective impedance seen at the input(s) of each corresponding stage of the matching system shown in Figure 1. Each plot shows a region of the impedance plane that input impedances of a given stage may exhibit as operating conditions vary.

the effective impedance ranges seen at the input(s) of each corresponding stage. A key element of the system is a resistance compression network, or RCN, [6], [14]–[16], which is a specialized matching network that losslessly transforms the impedance presented by multiple matched but variable resistive loads into a single, nearly-constant input resistance. This stage is represented by the leftmost block in Figure 1, and the range of impedances seen at the input of this stage is illustrated in the leftmost plot in Figure 2. The RCN’s ability to transform the widely varying resistances of a set of two (or more) matched loads into a single narrow-range driving-point resistance is central to the operation of the system.

The structure of the proposed matching system is selected based on the attributes of the RCN. Since the RCN requires multiple matched resistive loads to achieve narrow-range input resistance, the plasma drive coil stage comprises multiple plasma coils which provide nearly identical but dynamically-varying driving-point impedances. As illustrated in the rightmost plot in Figure 2, and described in this section, the input impedances at the multiple drive coils vary over a wide range in effective resistance (from  $R_{L,\min}$  to  $R_{L,\max}$ ), and over a narrower range in reactance (from  $X_{L,\min}$  to  $X_{L,\max}$ ). A tuning and impedance transformation stage, represented by the middle block in Figure 1 and the middle plot in Figure 2,

uses frequency tuning to null the reactive components of the plasma coil input impedances, yielding a set of widely varying but matched resistive impedances. This stage also provides impedance transformation, resulting in a resistive load range suitable for the RCN.

We describe each of these stages, starting with the structure and operation of the resistance compression network (leftmost block of Figure 1), which provides near-constant resistive input impedance but requires multiple loads. Next, we describe the plasma drive coil stage (rightmost block of Figure 1) which provides a means to realize the multiple matched load impedances at the plasma coils. Lastly, we describe the tuning and impedance transformation stage (middle block of Figure 1) which nulls the reactive component of the plasma coil impedances and transforms the resistive components to be compatible with the RCN.

#### A. Resistance Compression Network

A key component of the plasma matching system is the resistance compression network (RCN). As described in [6], an RCN is a special single-input multi-output matching network. Figure 3 shows two possible realizations (with a ground-referenced and differential input impedance in 3(a) and 3(b),

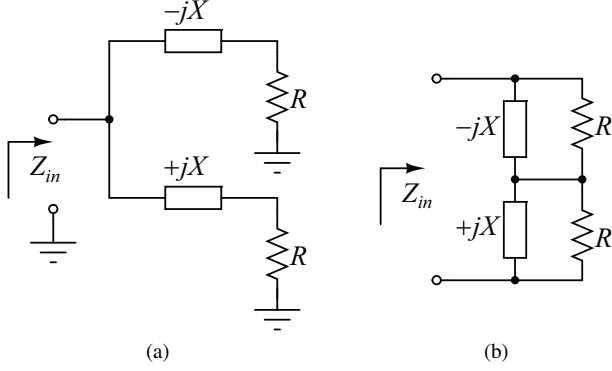


Fig. 3. Structure of two basic RCN topologies. The input impedance  $Z_{in}$  is resistive and is given by: (a)  $Z_{in} = \frac{X^2}{2R} \left[ 1 + \left( \frac{R}{X} \right)^2 \right]$ , and (b)  $Z_{in} = \frac{2R}{1 + (R/X)^2}$ .

respectively). The RCN utilizes resonant impedance transformation to losslessly transfer energy from a single input port to a pair of output ports loaded with identical resistances (which we refer to as a matched pair of loads), such that the resistance looking into the input port varies much less than the matched load resistances [6], [14]. Thus, the variation of the input resistance appears “compressed” as compared to the resistance variation of the matched loads. The matched loads ideally see equal portions of the input power, and the relative phases of the load voltages vary as the matched load impedances vary.

Consider the RCN of Figure 3(a), with its characteristic impedance value  $X$  chosen to be at the geometric center of the resistive load range,  $R_0$ . If the two matched loads  $R$  vary together about a nominal resistance  $R_0$ , from  $R_1 = R_0/b$  to  $R_2 = bR_0$ , the resulting impedance observed at the input of the RCN will be purely resistive across the entire RCN load range, and will vary from  $R_0$  to  $kR_0$ , where  $k = (1 + b^2)/2b$ . This is illustrated in Figure 4, which shows the variation in input impedance  $Z_{in} = R_{in}$  of the RCN of Figure 3(a) as a function of its matched load impedance  $R$ . (Note that  $b = \sqrt{R_2/R_1}$ , which represents the extent over which the matched loads vary. In addition,  $b$  determines  $k$ , which represents the extent of input resistance variation). For the highest degree of compression in the input impedance to be achieved, the geometric center of the matched load resistance range  $R_0$  should be equal to the RCN characteristic impedance  $X$ .

In an impedance matching system, such the one shown in Figure 1, the input impedance is typically desired to be as close as possible to some desired resistance value  $R_d$  (e.g., 50  $\Omega$ ). For a given RCN load range  $[R_1, R_2]$ , we can compute  $b = \sqrt{R_2/R_1}$ , and thus  $k$  can be determined. The RCN characteristic impedance  $X$  can be chosen to produce a compressed input resistance range between  $R_d - \Delta$  and  $R_d + \Delta$ , as illustrated in the leftmost plot of Figure 2. This can be accomplished by choosing  $X = 2R_d/(k + 1)$ , resulting in  $\Delta = (k - 1)R_d/(k + 1)$ . The nominal RCN load resistance is computed as the geometric mean of the minimum and maximum resistance values in the given RCN load range, i.e.  $R_0 = \sqrt{R_1 R_2}$ . Achieving this is one of the functions of the

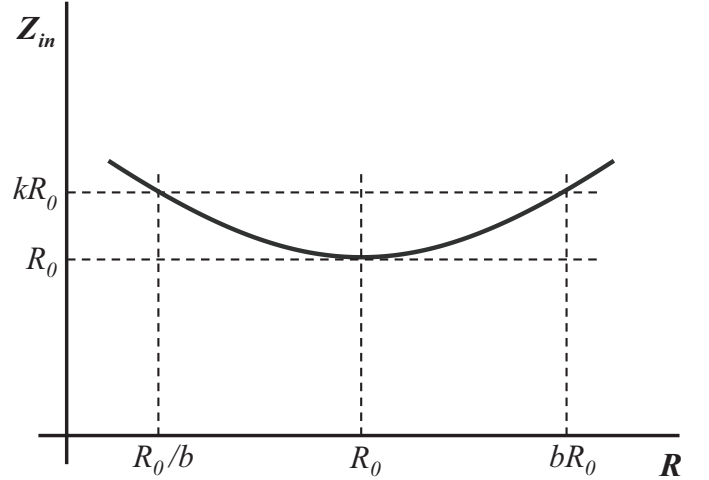


Fig. 4. Variation of the input impedance  $Z_{in} = R_{in}$  of the RCN in Figure 3(a) as a function of the load resistances  $R$  (log scale), when  $X = R_0$ .

tuning and impedance transformation stage described later in this section. Alternatively, to provide greater flexibility in the impedance levels selected for the RCN stage, it is possible to add an additional impedance transformation stage between the RCN and the input or to choose other RCN structures that can simultaneously provide both transformation and compression [6].

### B. Plasma Drive Coils

To utilize resistance compression to achieve impedance matching, one requires multiple loads which ideally are resistive and matched in impedance, though they may vary together over a wide range. Thus, a key element of the proposed approach shown in Figure 1 is two (or more) plasma drive coils that can drive the plasma while ideally acting as *independent* and *matched* loads that vary in impedance together across operating conditions (e.g., as the state of the plasma changes). Here we first describe the input impedance seen by a given drive coil in an ICP system, and then describe how we realize two drive coils that provide (ideally) identical input impedances (as required for the resistance compression system).

In a plasma system, the impedance seen at the terminals of a drive coil is a function of the power absorbed by the plasma as well as plasma composition, pressure, temperature and other conditions [5]. The plasma coil system can be modeled as a transformer, with the drive coil in the primary side, and the plasma load in the secondary [2], as shown in Figure 5(a). The voltage-current relationships for this network can be written as follows:

$$\begin{bmatrix} \tilde{V}_{rf} \\ \tilde{V}_p \end{bmatrix} = j\omega \begin{bmatrix} L_{11} & L_M \\ L_M & L_{22} \end{bmatrix} \begin{bmatrix} \tilde{I}_{rf} \\ \tilde{I}_p \end{bmatrix}, \quad (1)$$

$$\tilde{V}_p = -R_p \tilde{I}_p, \quad (2)$$

where  $L_{11}$  and  $L_{22}$  denote the drive coil and the plasma load self-inductances, respectively,  $L_M$  denotes the mutual

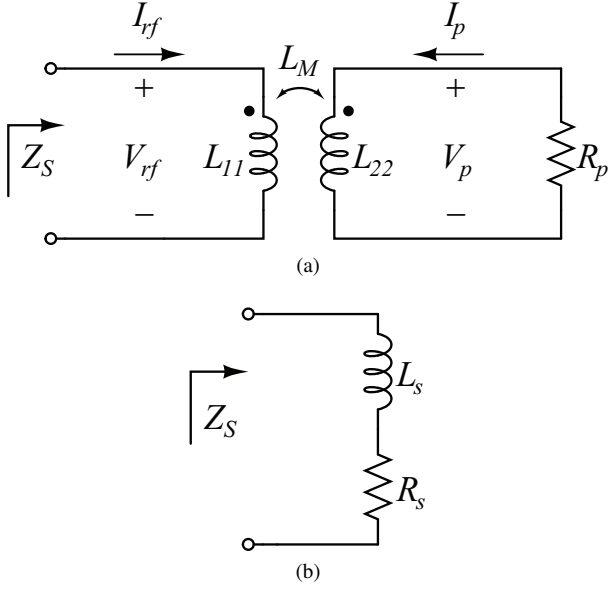


Fig. 5. Circuit models for a plasma drive coil [2]. (a): Transformer model with the drive coil on the primary side, and the plasma load on the secondary; (b) effective plasma drive coil impedance seen at its terminals. The inductance  $L_s$  is due to the coil's self-inductance as well as the plasma inductance, and  $R_s$  is a combination of the coil resistance and the plasma resistance. The values of both parameters can change with the plasma operating conditions.

inductance between the drive coil and the plasma, and  $R_p$  denotes the plasma resistance. Equations (1) and (2) can be combined to obtain an expression for the effective input impedance  $Z_S$  as seen from the terminals of the plasma coil:

$$Z_S = \frac{\tilde{V}_{rf}}{\tilde{I}_{rf}} = \frac{\omega^2 L_M^2 R_p}{R_p^2 + \omega^2 L_{22}^2} + j\omega \left( L_{11} - \frac{\omega^2 L_M^2 L_{22}}{R_p^2 + \omega^2 L_{22}^2} \right) \quad (3)$$

Equation (3) can be further simplified by using the fact that in ICP discharge systems, the skin depth of the plasma is typically much smaller than the radius of the plasma chamber [2], which results in  $\omega^2 L_{22}^2 \gg R_p^2$ , yielding:

$$Z_S \approx \left( \frac{L_M}{L_{22}} \right)^2 R_p + j\omega \left( L_{11} - \frac{L_M^2}{L_{22}} \right) \quad (4)$$

Therefore, the effective impedance seen at the coil terminals of a single plasma drive coil can be represented as shown in Figure 5(b). The effective series resistance  $R_s$  depends on the plasma resistance  $R_p$ , the inductive coupling between the coil and the plasma, and the coil's resistance, and can vary over a substantial range (e.g., 10:1 depending on the operating conditions). Similarly, the reactive component of the load impedance represented by inductance  $L_s$  depends on the coil's self-inductance, mutual inductance, as well as the plasma inductance. The rightmost plot in Figure 2 illustrates the corresponding impedance range seen at the input of a drive coil for this stage, and depicts the resistive and reactive impedance variation.

It is important to note that the loads seen by each branch of the RCN should (ideally) be matched but uncoupled (i.e., the voltage at one load does not depend on the current into the other load). If the coils are coupled, then the RCN circuit

may no longer compress the plasma resistance in the expected manner. Likewise, not only is mutual inductance relevant, any mutual resistance among coupled coils would be of concern [17].

To address this need for uncoupled, nominally identical loads, we utilize multiple plasma drive coils that should ideally fulfill two conditions: (a) the coils should have similar self-inductances and provide low magnetic coupling to each of the other coils (ideally uncoupled); and (b) each coil should drive plasma having substantially the same conditions, such that the coils have similar driving-point impedances. This is ideally provided by having the multiple coils drive the same physical region of plasma. Together, these conditions lead to a set of coils providing identically varying load impedances.

There are many coil geometries that can provide one or both of the aforementioned conditions. A preferred construction for the multiple coils is an implementation in which the coils are magnetically uncoupled (magnetically "orthogonal") but spatially close (such that they drive similar or identical portions of the plasma). This can be accomplished with coils that physically overlap the same space and drive similar (or the same) plasma volume, but are wound such that net flux from each coil does not link the other coil(s). One way to implement this is to make the windings overlapped but geometrically orthogonal, as illustrated in Figure 6. (The desired requirements can be achieved, for example, by placing the coils with the same center but rotated by 90 degrees). A particular implementation using the design approach illustrated in Figure 6 is described in Section III below.

### C. Tuning and Impedance Transformation

We now consider the design of the middle stage in the system of Figure 1, which provides reactive tuning and impedance transformation. The ICP coil design illustrated above yields two plasma coils having ideally matched driving point impedances. As illustrated in the rightmost plot of Figure 2, the coil impedances can vary together over a wide range in resistance, but can also vary together over a narrow range in reactance as operating conditions change. The loads for the RCN stage should ideally be purely resistive, however, as was explained in Section II(A). A first function of the tuning and impedance transformation stage in Figure 1 is to provide reactive tuning to null the reactive component of the drive coil impedances. A second function of this stage is to provide impedance transformation such that the RCN stage can operate at a desired impedance level.

As explained in the previous section and illustrated in the rightmost plot of Figure 2, the plasma coil impedance consists of resistive and reactive portions. As a practical matter, the inductance provided by the plasma coil can vary somewhat across operating conditions (e.g., owing to the screening out of the RF fields from the interior of the plasma chamber as the plasma density increases [5]). This is depicted in Figure 2 as reactive variation between  $X_{L,\min}$  and  $X_{L,\max}$ . To address this, we employ narrow-band *dynamic frequency tuning*, whereby small variations in the system operating frequency are used to adaptively tune the system such that the input impedances at

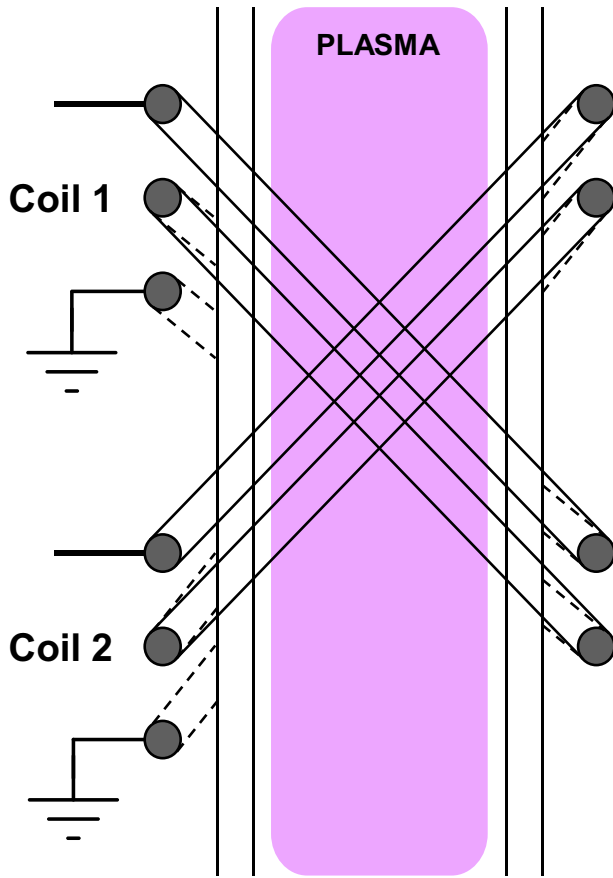


Fig. 6. Two coils can be wound around the same chamber such that they are spatially orthogonal while exciting the same physical plasma region. This results in two magnetically uncoupled coils with matched driving-point impedances.

the second stage appear substantially resistive, as illustrated in the middle plot of Figure 2. To accomplish this, a tuning network is used for each coil. In its simplest form, this can be a capacitor placed in series with each coil. The capacitor is selected to null the reactive component of the net impedance at some nominal operating point. Modest adaptation of the operating frequency then enables a net resistive input impedance to be maintained in the face of variations in coil inductance.

In some designs, the frequency selectivity of a capacitor in series with the plasma coil enables frequency tuning to be utilized with only small variations in frequency. In cases where a higher degree of frequency selectivity is desired (e.g., for a narrower frequency tuning range), a more sophisticated tuning network can be used. For example, one might add a series-resonant network in the tuning stage to make the resistive tuning point more highly frequency selective, as illustrated in Figure 7. In this manner, the coil tuning can be made far more frequency selective than other elements of the system, so that the small frequency adjustments for nulling coil reactance do not substantially disturb other system aspects.

Consider the use of the circuit implementation in Figure 7 for dynamic frequency tuning. The circuit branch in Figure 7(a) shows the effective impedance of a plasma coil in series with two functional blocks (shown in red and green). The red block consists of a capacitance  $C_R$  which cancels the average

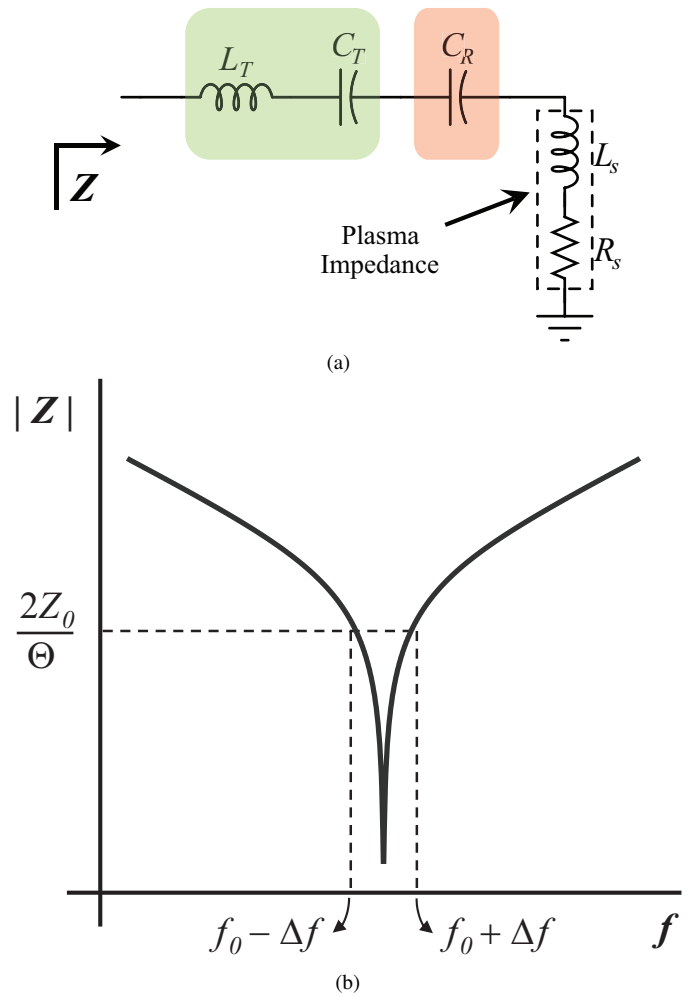


Fig. 7. Illustration of dynamic frequency tuning. (a): Plasma impedance in series with two functional blocks (red and green). The red block (consisting of  $C_R$ ) tunes out the average bulk plasma coil reactance. The green block ( $L_T$  in series with  $C_T$ ) is used to make the reactance very frequency selective, such that narrow-band frequency tuning can be used to achieve resistive loading of the RCN stage; (b): Plot showing the effect of small frequency adjustments  $\Delta f$  from the nominal operating frequency  $f_0$  on the maximum achievable reactance.  $Z_0$  is the tank characteristic impedance, and  $\Theta = f_0/\Delta f$ .

bulk plasma coil inductance. If the plasma coil inductance were constant across operating conditions, the resulting net impedance would be resistive, and no further action would be required. However, since the inductance does change, it needs to be nulled dynamically. The network comprising  $C_R$  and  $L_s$  is frequency selective, allowing for dynamic frequency tuning. Adding in  $L_T$  and  $C_T$  (tuned resonant at a nominal point) increases the  $Q$  of the net series network, further increasing frequency selectivity.

Figure 7(b) illustrates the effect of utilizing small frequency adjustments  $\Delta f$  about the nominal operating frequency  $f_0$ . Depending on the allowed range of frequency adjustment,  $\Theta \equiv f_0/\Delta f$  (typically  $\gg 1$ ) can be set, and the tank's characteristic impedance  $Z_0$  can then be selected to provide the desired maximum amount of reactance cancellation. The result of the two functional blocks in Figure 7(a) is a net impedance that is dynamically tuned to be resistive (though still variable; the resistive variation is treated by the RCN stage). This effect

is depicted ideally as a flattening of the impedance region on the impedance plane, i.e., the  $[X_{L,\min}, X_{L,\max}]$  variation range at the input of the plasma coil gets ideally flattened to 0, as illustrated in the middle plot of Figure 2.

A second function of the intermediate stage in Figure 1 is to transform the reactance-compensated plasma load impedance to a desired range over which the RCN is designed to operate. This can be accomplished with a variety of circuit implementations (e.g., utilizing transformers, transmission-line transformers [18], immittance converters [19] or other transformation networks that function well with variations in loading impedance). As was discussed in Section II(A), for the RCN to achieve maximum compression in input impedance, a specific RCN nominal load resistance  $R_0$  is imposed (which must be equal to the RCN characteristic impedance  $X$ ). Thus, for maximum compression, the RCN matched loads should vary from  $R_0/b$  to  $bR_0$ . As can be seen in the middle and rightmost plots of Figure 2, the plasma coil resistive variation range should ideally be transformed from  $[R_{L,\min}, R_{L,\max}]$  into  $[R_0/b, bR_0]$  in order for it to be maximally compressed by the RCN. The result of this is a matched pair of resistive load impedances that can be compressed into a narrow range by the RCN.

Note that it is possible to switch the order of the RCN and the impedance transformation stages in Figure 1 to achieve the desired match. Moreover, it is also possible to add another impedance transformation stage in front of the RCN to step-up or step-down the RCN-compressed resistive input impedance as required. Likewise, as will be illustrated in the next section, the functional elements of the different blocks in Figure 1 can in some cases be combined together, providing reduced component count and increased power efficiency. Together, these stages enable energy transfer into the plasma while presenting a narrow-range input impedance for the RF power amplifier.

### III. MATCHING NETWORK DESIGN AND IMPLEMENTATION

In order to validate the proposed approach, a prototype dynamic matching system was implemented and tested in a low pressure ICP application. The design target is to deliver up to 250 W at a nominal frequency of 13.56 MHz into a 3.25 inch-diameter plasma chamber. Figure 8(a) shows the notional circuit schematic of the matching network including all of the described functions, while Figure 8(b) shows the actual implementation with components combined to simplify the system. Detailed component selections for the prototype system are listed in Table I.

The plasma drive coil subsystem comprises two coils wound on a fixture using the orthogonal structure illustrated in Figure 6. The fixture is shown in Figure 9, and is designed to mount around the cylinder of the plasma chamber. The custom-made Delrin base of the fixture has a 3.25 inch hole that allows the fixture to slide onto the plasma chamber, and a set of grooves machined to provide space for the pair of orthogonal two-turn windings. Two Teflon strips threaded with 100 mil wide and 50 mil deep T-slot grooves (which were made with a micro-slitting saw with a cutting diameter of 93 mil and

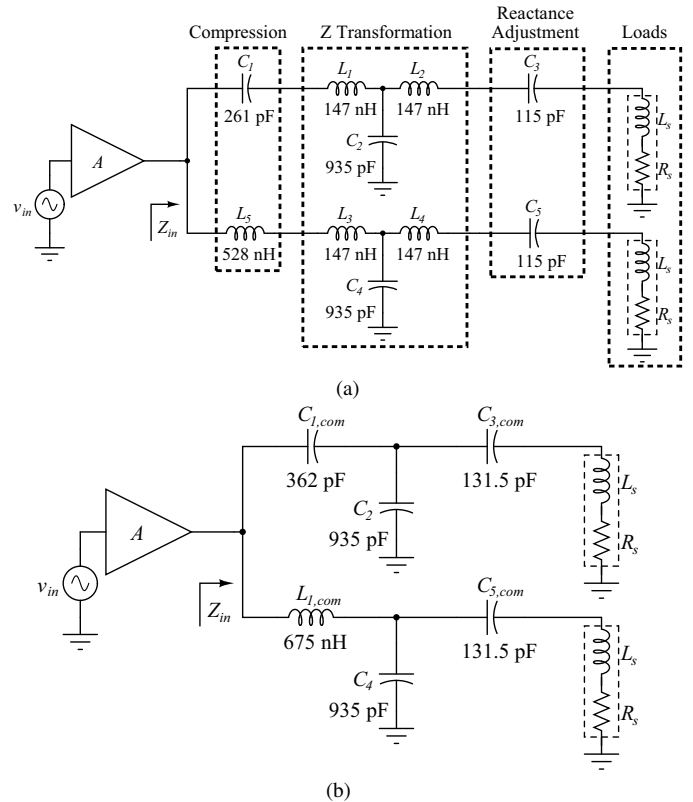


Fig. 8. Design of the matching network. (a): A conceptual illustration showing the different circuit blocks of the structure in Figure 1, (b): The actual implementation of the matching system in which a number of the conceptual elements of (a) are combined together. Detailed component selections are listed in Table I.

30 mil saw thickness) are fixed on the Delrin base; these allow the two-turn coils to be wound tightly and consistently around the chamber, and provide thermal insulation between the wires and the Delrin fixture as well as electrical insulation between the turns. (Electrical insulation is desirable as peak RF voltages applied to the plasma coils may exceed 1 kV). The two two-turn coils are each wound with about 17 inches of 92 mil  $\times$  25 mil rectangular cross-section wire; a layer of Kapton tape and a turn-to-turn spacing of 100 mil are used to prevent any arcing between the turns. Under this configuration, the self-inductance of each coil was around 1.2  $\mu$ H, the mutual inductance between the orthogonal coils as well as the capacitive coupling effects were found to be negligible.

Based on measurements of the coil impedance when the system was powered off, as well as on prior characterization of our particular experimental setup, the prototype matching network was designed for a plasma drive coil impedance range (see Figure 2) that is estimated to vary resistively between  $[R_{L,\min}, R_{L,\max}] = [1.7 \Omega, 7 \Omega]$ , and reactively between  $[X_{L,\min}, X_{L,\max}] = [j97 \Omega, j102 \Omega]$ .

The network in Figure 8(a) is a conceptual illustration showing the different circuit blocks in the high-level structure in Figure 1.  $C_3$  and  $C_5$  are implemented with P90 ceramic capacitors, and are selected to tune out the coils' reactances at the nominal operating frequency, 13.56 MHz, when there is no plasma in the chamber. These capacitors serve to cancel

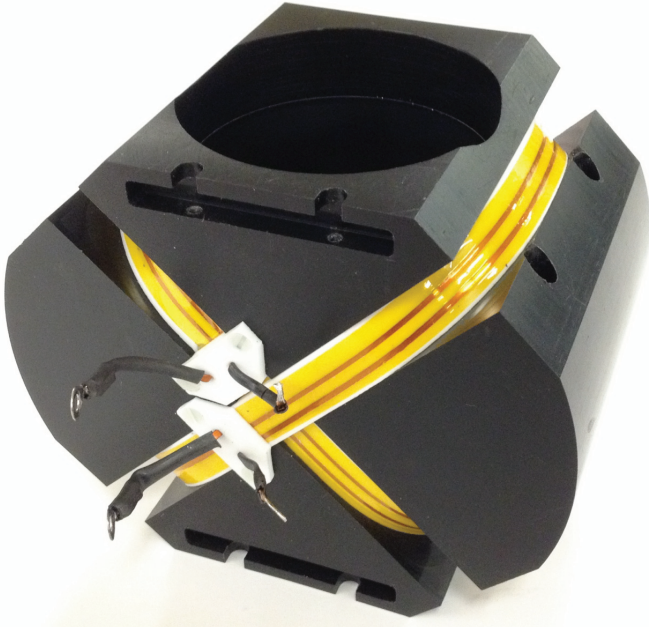


Fig. 9. Fixture used to realize the orthogonal coil structure. This makes the wires easily accessible and holds them in place. The Teflon strips (white) help thermally insulate the wires from the Delrin fixture (black) and - together with kapton tape - also provide added electrical insulation.

the bulk plasma coil reactance (i.e., they play the role of the red block with  $C_R$  in the illustration in Figure 7(a)). The choice of these capacitors can also allow for cancellation of any reactive mismatch between both plasma loads due to network implementation non-idealities and small differences in the coil implementation and geometry. Furthermore, capacitors  $C_3$  and  $C_5$ , each in series with the effective plasma drive coil inductance  $L_s$ , also form a pair of high-Q series-resonant tanks. This allows one to control the effective reactance in each branch (capacitively or inductively) by narrow-band frequency modulation. For this design, a maximum allowed frequency adjustment  $\Delta f$  was imposed to be 5% of the nominal operating frequency  $f_0 = 13.56$  MHz, yielding  $\Theta = f_0/\Delta f = 20$ . The resulting tank characteristic impedance  $Z_0$  in each branch is close to  $100 \Omega$ , and thus each tank can provide a reactance compensation range of  $\pm j10 \Omega$ , which is sufficient for this design. It is therefore not necessary to add the green block shown in Figure 7(a) for this particular design.

In this system, the frequency selectivity of the output resonant tank (e.g.,  $C_3$ ,  $L_s$ ,  $R_s$  in Figure 8(a)) is much larger than that of the RCN. It is owing to this high frequency sensitivity of the output narrowband tanks (as compared to the RCN and transformation networks) that the operating frequency can be exploited to adjust the tuning of the coils for resistive operation across the plasma regions of operation. While this dynamic frequency tuning is implemented manually in the present prototype, it can be implemented in a closed-loop control strategy that dynamically selects the optimal power amplifier operating frequency for which the reflection is minimal. As a side note, the high quality factor of the output resonant tank also makes it sensitive to any parasitic capacitance from the center point of the series resonant network to earth; this needs

careful attention in the physical implementation.

The RCN stage is designed to compress a resistance variation about a nominal value of  $R_d = 50 \Omega$ . For the estimated plasma load resistance range, the multiplicative factor  $b = \sqrt{R_{L,\max}/R_{L,\min}}$  (refer to Section II(A)) is about 2, which results in  $k = 1.25$ . Thus, according to the description in Section II(A), the RCN characteristic impedance (which is the reactance of the RCN components at the operating frequency of 13.56 MHz) is selected as  $X = 2R_d/(k+1) = 45 \Omega$ . This yields the values of  $C_1$  and  $L_5$  shown in Figure 8(a). The geometric mean of the plasma loads  $R_{L,\min}$  and  $R_{L,\max}$ , given by  $\sqrt{R_{L,\min}R_{L,\max}}$ , is around  $3.45 \Omega$ . To maximize compression at the RCN input, a nominal resistance  $R_0 = X = 45 \Omega$  seen at the output of each RCN branch is imposed. This means that the resistance range to be compressed by the RCN must vary between  $R_0/b$  and  $bR_0$ , namely  $22.5 \Omega$  and  $90 \Omega$ . Thus, an impedance transformation stage is needed between the plasma drive coils and the RCN stage.

In this prototype design, the impedance transformation stage is implemented using T-network immittance converters, as shown in Figure 8(a). Each T-network is designed to transform the range of plasma resistance into the range required by the RCN for it to compress effectively. An immittance converter [19] transforms a load resistance  $R$  into a resistance of value  $X_{im}^2/R$ , where  $X_{im}$  is the characteristic reactance of the network at the operating frequency. The geometric mean of the plasma load resistance,  $3.45 \Omega$ , needs to be stepped up to  $R_0 = 45 \Omega$ , which results in  $X_{im} = 12.5 \Omega$ . This reactance corresponds to the values of  $(L_1, L_2, C_2)$  in the top branch and  $(L_3, L_4, C_4)$  in the bottom one.

In the actual implementation, the conceptual elements (and stages) of Figure 8(a) are combined together, resulting in the greatly simplified circuit of Figure 8(b). A photograph of the implemented circuit is shown in Figure 10, and Table I shows the details of the selected components for the network. Note that the network is shielded in a custom enclosure, with appropriate points insulated to prevent arcing. High-voltage N (HN) connectors are used at the outputs to the plasma coils owing to the high RF output voltages of the system.

To illustrate the value of utilizing frequency-based reactance compensation along with the resistance compression, we model the expected driving point impedance for our system in Figure 8(b) with and without frequency tuning, and plot it on a Smith Chart normalized to  $50 \Omega$ . Figure 11(a) shows the modeled input impedance (shown in blue) of the matching network corresponding to a simulated load range that varies resistively between  $1 \Omega - 10 \Omega$ , and reactively between  $j97 \Omega - j102 \Omega$ . Even though the resistive variation is compressed by the RCN, it can be seen that even a small reactive variation can have a drastic effect on the input impedance, resulting in reflected powers exceeding 10%. Figure 11(b) shows the result when the operating frequency is dynamically adjusted by no more than 5% of the nominal operating frequency of 13.56 MHz to null the reactive loading component to the RCN. It is evident that this narrowband frequency adjustment significantly reduces the input impedance variation, and yields a simulated worst-case reflected power ratio close to 8% (i.e., no more than 8% of the RF input power gets reflected back).

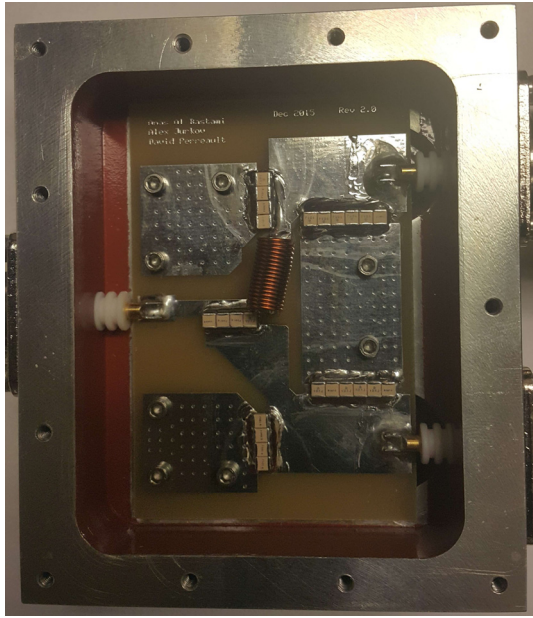


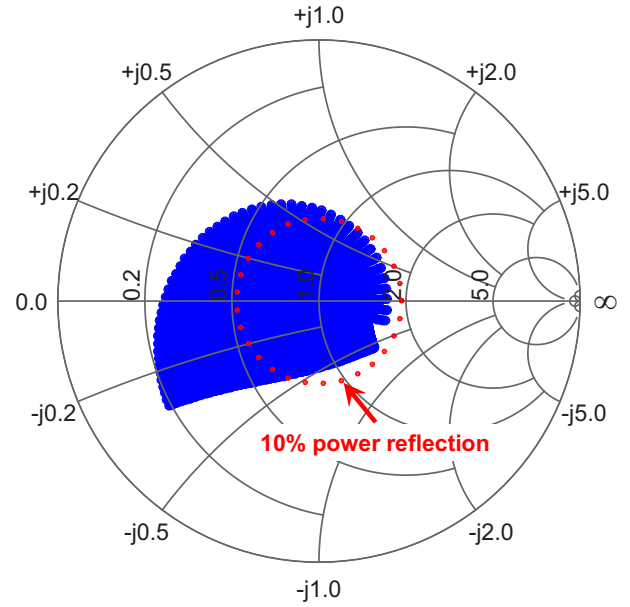
Fig. 10. Photograph of the circuit in Figure 8(b).

TABLE I  
COMPONENT VALUES FOR THE MATCHING SYSTEM IN FIGURE 8(B)

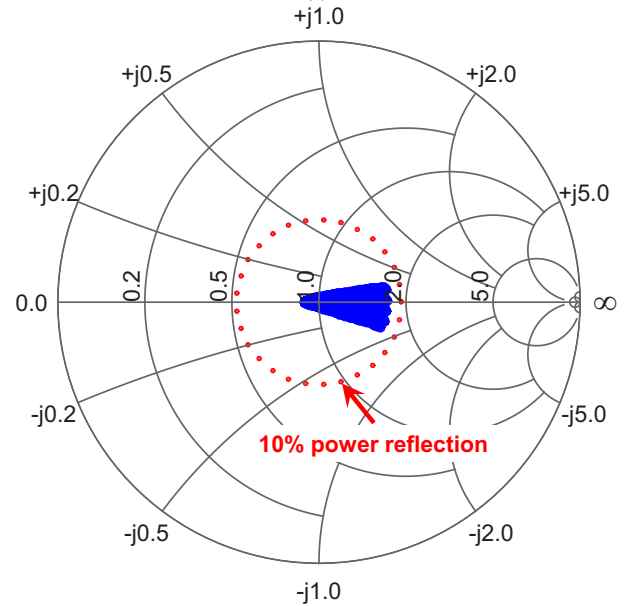
Component	Value	Implementation
$C_{1,com}$	261 pF	500 V P90 ceramic capacitors (ATC100B, ATC Corp.)
$L_{1,com}$	675 nH	15 turns of 20 AWG wire, ID = 335 mil
$C_2$	935 pF	500 V P90 ceramic capacitors (ATC100B, ATC Corp.)
$C_4$	935 pF	500 V P90 ceramic capacitors (ATC100B, ATC Corp.)
$C_{3,com}$	131.5 pF	1.5 kV NP0 ceramic capacitors (VJ1111D, Vishay Intertechnology, Inc.)
$C_{5,com}$	131.5 pF	1.5 kV NP0 ceramic capacitors (VJ1111D, Vishay Intertechnology, Inc.)
Input connector	-	HN-type 50 $\Omega$ panel mount solder cup connector
Output connectors	-	HN-type 50 $\Omega$ panel mount solder cup connector

#### IV. EXPERIMENTAL RESULTS

The etching system used for the experiments described here was a custom-built, ICP-Reactive Ion Etching (RIE) reactor designed for etching small substrates (1-2 inch diameter). The reactor was built as part of an effort to produce high performance yet ultra-low capital cost semiconductor equipment for low throughput applications found often in academia, early-stage businesses, and corporate R&D [20]. The reactor chamber consists of a 3 inch ID alumina ( $Al_2O_3$ ) cylinder sealed on top and bottom to standard Conflat-style vacuum flanges. The top flange includes a gas showerhead for providing a spatially uniform distribution of the desired process gas to the chamber. This showerhead is fed from an external gas block assembly containing a bank of mass flow controllers and an electronically-controllable valve manifold. The bottom flange mates to a lower chamber assembly that



(a)



(b)

Fig. 11. Simulated input impedance (blue) of the designed RCN in Figure 8(b) plotted on a Smith Chart normalized to 50  $\Omega$ . A modeled load impedance was set to vary resistively between 1  $\Omega$ –10  $\Omega$ , and reactively between  $j97 \Omega$ – $j102 \Omega$ . (a): No adjustment to the operating frequency was performed, (b): Operating frequency dynamically adjusted by up to 5% of its nominal value of 13.56 MHz.

contains a port for the vacuum foreline and a differentially-pumped vacuum feedthrough for the substrate chuck assembly (which serves as the RIE electrode). The system is pumped down to a base pressure of  $\sim 5$  mTorr using a 2-stage rotary vane pump. Due to the small overall size of the reactor ( $< 2$  L) and the small gas flows used ( $< 10$  standard cubic centimeters per minute), this rotary vane pump can easily maintain the 20-50 mTorr operating pressures needed for the dry etching processes performed. The substrate chuck assembly contains connections for the RIE bias power (0-5 W at 13.56 MHz), substrate cooling, temperature measurement, and a clamping

system to register and confine the wafer being etched. The entire chuck assembly can be translated up and down within the reactor chamber via the differentially pumped feedthrough to achieve the desired spacing between the plasma generation region (the region spanned by the orthogonal coils, see Figure 6) and the substrate. The etching results shown below used a spacing of 7.5 inches between the center of the coils and the substrate.

The results shown here are for generating plasmas using  $O_2$ ,  $C_4F_8$ , and  $SF_6$  gases, which are commonly used in plasma ashing, passivation, etching, among other processes, at a low pressure of about 20 mTorr. An ENI 3100LA RF power amplifier was used to drive the ICP system at a nominal frequency of 13.56 MHz (with frequency variations over a range of 13.56-14.04 MHz to allow dynamic tuning cancellation of the coil reactances). Power was gradually increased from zero to about 230 W (280 W for  $SF_6$ ), and a Bird 4421 RF power meter was used to record the forward and reflected powers at the output of the RF power amplifier, in order to gauge the degree to which desired performance of the RCN-based matching system is achieved. Our metric in this experiment is the ratio of power reflected from the load to forward RF power. This power reflectance would ideally be zero. When the input impedance of the dynamic impedance matching system is  $50\Omega$ , it is matched to the power amplifier's output impedance, no power is reflected, and the power capability of the power amplifier is used effectively. In this experiment, the aforementioned frequency tuning strategy was utilized to adjust the match to the plasma. At each power level, the operating frequency was manually adjusted to obtain the lowest measured reflected power. For each gas, the ratio of the reflected power to the forward power was recorded, as shown in Figure 12. It can be seen that less than 7% of the power was reflected back in all three gases, indicating an acceptable matching behavior across the entire plasma range of operation, which included both E-mode and H-mode drive of the plasmas. Figure 13 shows the plasma system being powered by the orthogonal coils.

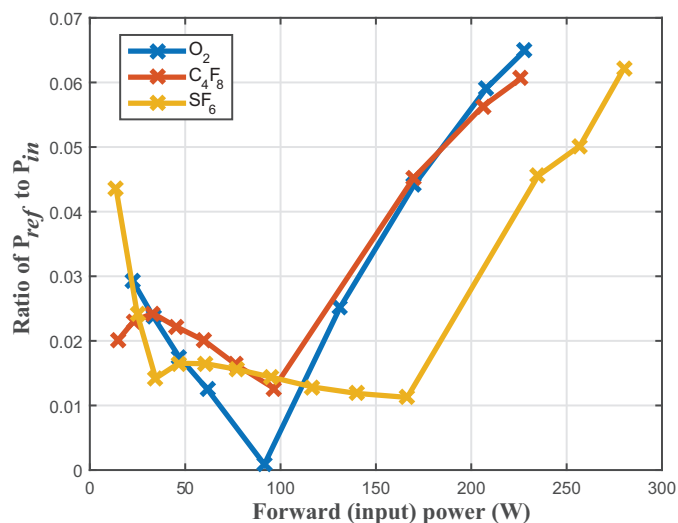


Fig. 12. Result showing the ratio of reflected power to input power, plotted across the entire range of plasma operation.

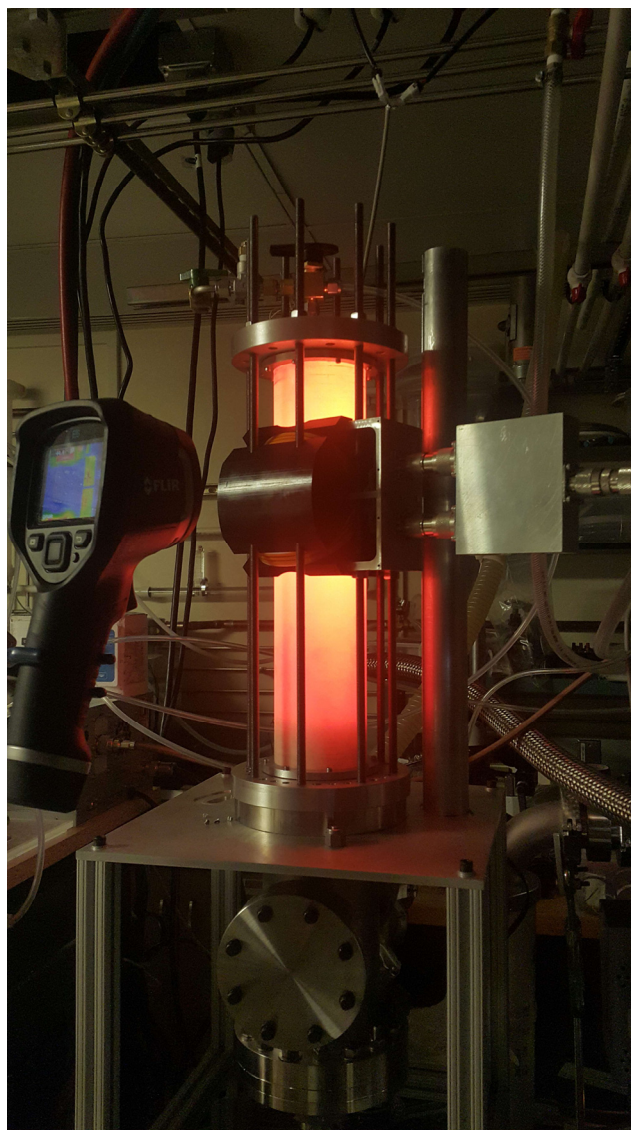


Fig. 13. The proposed plasma drive system with  $O_2$  being ionized during a plasma ashing process. The orthogonal coils on the plasma chamber can be seen in the center of the photograph, with the single-input two-output matching system in the sealed enclosure to its right.

The next experiment was used to demonstrate that the plasmas generated using the prototype matching system at these power levels have enough energy and are dense enough to perform useful processes on a silicon wafer. Figure 14(a) shows a 650-675  $\mu\text{m}$  thick silicon wafer obtained for this experiment.

A 10  $\mu\text{m}$  thick photoresist layer was patterned on top of it using photolithography techniques, with a horizontal gap width of 100  $\mu\text{m}$ , shown in Figure 14(b). The experiment started by flowing 5 standard cubic centimeters per minute (sccm) of  $O_2$  at 200 W for about 10 minutes to clean the chamber from any impurities that might affect the wafer. Next, the wafer in Figure 14(b) was placed and 6 sccm of  $SF_6$ , the primary gas used for etching, was allowed to flow into the chamber for 10 minutes at 250 W. The result of this step is the isotropically-etched wafer shown in Figure 14(c). The depth of the etch

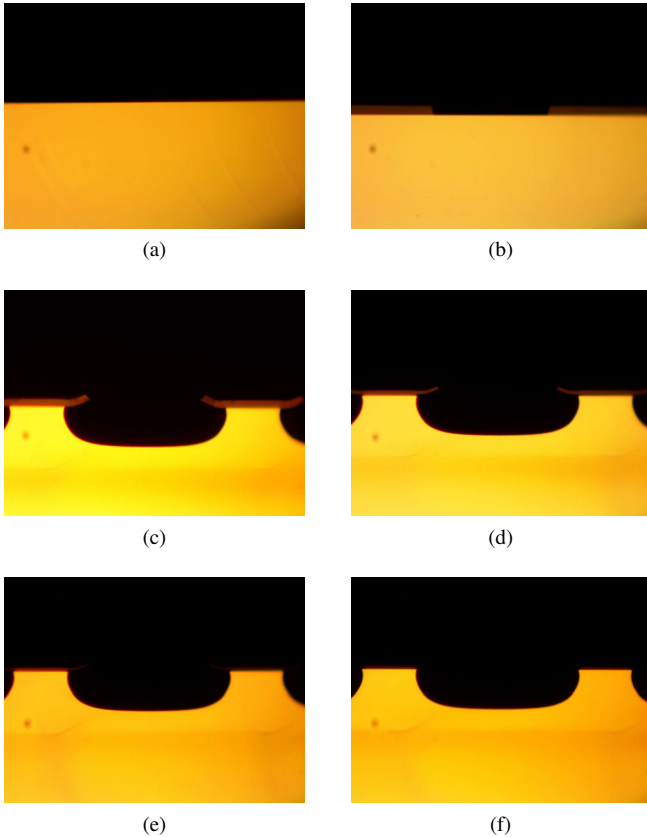


Fig. 14. Photograph of the wafer cross section (a) before processing it; (b) after adding a patterned photoresist layer; (c) after etching with  $\text{SF}_6$  for 10 minutes; (d) after ashing for 15 minutes; (e) after ashing for 30 minutes; and (f) after ashing for 45 minutes.

after the 10 minutes was measured to be  $37 \mu\text{m}$ , giving a time-averaged etch rate of  $3.7 \mu\text{m}/\text{min}$ . This etch rate is comparable to results obtained in the same reactor [4] using traditional plasma generation and impedance matching systems, and is more than sufficient for many applications.

The etching step was followed by three rounds of 15-minute runs of  $\text{O}_2$  ashing, using 5 sccm of  $\text{O}_2$  at 200 W of power. Figures 14(d)-(f) show the result after each ashing run. It can be seen that the photoresist gradually gets thinner, until no noticeable traces of it are observed. It can be concluded that the proposed matched coil system can be effective in systems designed for semiconductor processing with plasmas.

## V. DISCUSSION

It can be seen that the proposed system clearly achieves a high degree of compression of the plasma coil impedances into a small impedance variation range, which results in acceptable levels of reflected power in a compact design. The results are in accordance with the modeled predictions for our system. The matching system is far smaller (over an order of magnitude smaller) than a conventional TMN, may be expected to be significantly less expensive, and also offers the opportunity for high-bandwidth control of the match.

However, given the fact that the RCN imposes an additional requirement of having multiple matched and independent plasma drive coils, it is natural to pose the question of how

well a simpler fixed two-port matching system could perform (i.e., one that does not require multiple plasma loads and thus that does not require a specialized winding structure such as the one in Figure 9). If such a fixed two-port matching network could be made to achieve low power reflectance across the plasma operating range, it could likewise offer small size, low cost and high bandwidth, while simplifying construction.

Appendix A provides analysis for the achievable performance of fixed two-port matching systems as well as a simulation for the calculated best two-port fixed matching system. The result is that with a simple implementation of the two-port network reactances (i.e., with each reactance implemented using a single inductor or capacitor), a simpler two-port matching system with a single plasma drive coil *cannot* achieve close to the same degree of compression that can be achieved by the proposed RCN-based matching system. This can be seen by comparing the results in Figures 11 and 15. It can be concluded that the proposed RCN-based system is thus superior to fixed two-port matching networks, while achieving small size and high simplicity as compared to tunable matching networks in this application.

## VI. CONCLUSION

A dynamic matching system for radio-frequency inductively-coupled plasma generation has been introduced. This system can provide efficient power delivery into plasma loads with good matching to the power amplifier, while achieving small size, low cost, fast control speed, and eliminating mechanical or switched components. The proposed approach utilizes a special set of matched but orthogonal drive coils along with a resistance compression network to compress the variable plasma impedance to an almost fixed value that results in minimal reflected power to the power amplifier. By arranging the plasma drive coils in special geometries such that they are largely magnetically uncoupled, and using dynamic frequency tuning to compensate for load reactance variations, the RCN-based matching system can be used to provide passive, high-bandwidth matching with no mechanically-controlled or moving parts. This can permit the design of efficient, compact, fast-response, and cost-effective plasma generation systems. An ICP discharge system utilizing this technique has been constructed and the results show good matching across the entire range of plasma operation for three gases commonly used in various semiconductor manufacturing processes:  $\text{O}_2$ ,  $\text{C}_4\text{F}_8$ , and  $\text{SF}_6$ . The results also demonstrate the ability of the plasma generated using the proposed matching system to perform etching and ashing on a silicon wafer.

## APPENDIX A

### ANALYSIS USING TWO-PORT NETWORKS

Given a load impedance range ( $Z = R + jX$ ), with a resistive part between  $R_{\min}$  and  $R_{\max}$ , and a reactive part between  $X_{\min}$  and  $X_{\max}$ , there are many possible fixed two-port passive networks that can transform this load impedance to some other desired value. To prevent power losses due to resistive elements, the network is required to consist of purely

reactive elements (e.g., inductors and capacitors). For example, it is possible to synthesize a lossless two-port matching network that transforms the load impedance  $Z$  to a desired input impedance  $Z_{in}$ .

The voltage-current relationships for a general lossless two-port network can be written as follows (note that lossless networks that contain only inductors and capacitors are also reciprocal, and their impedance matrix is thus symmetric):

$$\begin{bmatrix} \tilde{V}_1 \\ \tilde{V}_2 \end{bmatrix} = \begin{bmatrix} jX_{11} & jX_M \\ jX_M & jX_{22} \end{bmatrix} \begin{bmatrix} \tilde{I}_1 \\ \tilde{I}_2 \end{bmatrix}. \quad (5)$$

If port 2 of the network is terminated with load impedance  $Z$ , the terminal condition  $\tilde{V}_2 = -Z\tilde{I}_2$  is imposed, and the input impedance seen looking into port 1 becomes:

$$Z_{in} = jX_{11} + \frac{X_M^2}{jX_{22} + Z}. \quad (6)$$

The objective is to have  $Z_{in}$  equal to some desired reference impedance  $Z_0$  (e.g.,  $50\Omega$ ). The ratio of power reflected from the load to forward RF power is used as a metric to assess matching, and is given by  $|\Gamma_{in}|^2$ , where  $\Gamma_{in}$  is given by:

$$\Gamma_{in} = \frac{Z_{in} - Z_0}{Z_{in} + Z_0}, \quad (7)$$

where  $Z_0$  is the reference impedance, and is  $50\Omega$  in our case. One can, for instance, pick  $X_{11}$ ,  $X_M$ , and  $X_{22}$  at the operating frequency such that the peak reflected power, and thus  $|\Gamma_{in}|^2$ , across the entire load impedance range is minimized.

As an example, consider the load impedance range given in Figure 11, with  $R_{min} = 1\Omega$ ,  $R_{max} = 10\Omega$ ,  $X_{min} = j97\Omega$ , and  $X_{max} = j102\Omega$  at the operating frequency of 13.56 MHz. Using brute-force search techniques to select reactance values that minimize the worst case reflection ratio  $|\Gamma_{in}|^2$  across the impedance range yields the parameters  $X_{11} = j224\Omega$ ,  $X_M = j52\Omega$ ,  $X_{22} = -j88\Omega$ . The resulting input impedance is shown on a Smith Chart in Figure 15(a). It can be seen that the reactive variation of the output load results in reflected power ratios that significantly exceed 10% for much of the load range. If the reactances of the optimal two-port network are each implemented simply with a single inductor or capacitor, and 5% narrowband frequency adjustment is utilized, the resulting input impedance is shown in Figure 15(b). It can be seen that in this case, the reflected power ratio cannot be maintained to be less than 10%. Note, however, that there might be alternative implementations of the network that have better frequency behavior, at the expense of increased component count. Alternatively, one can also move to three-port networks, such as the RCN described in the paper.

#### ACKNOWLEDGMENT

The authors would like to thank the Qatar Foundation Research Division for their financial support of author Anas Al Bastami. The authors also acknowledge the support of the MIT Center for Integrated Circuits and Systems.

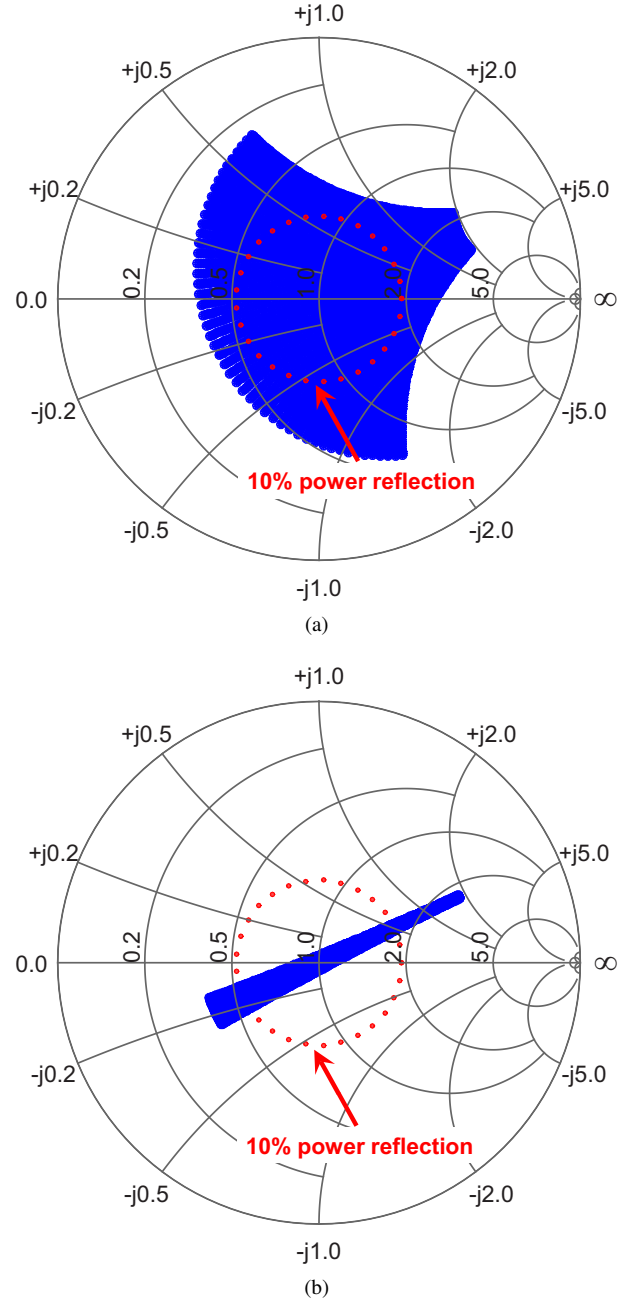


Fig. 15. Simulated input impedance (blue) of the optimal two-port network plotted on a Smith Chart normalized to  $50\Omega$ . A modeled load impedance was set to vary resistively between  $1\Omega - 10\Omega$ , and reactively between  $j97\Omega - j102\Omega$ . (a): No adjustment to the operating frequency was performed, (b): Operating frequency dynamically adjusted by up to 5% of its nominal value of 13.56 MHz.

#### REFERENCES

- [1] National Research Council, *Plasma Processing of Materials: Scientific Opportunities and Technological Challenges*. Washington, DC: The National Academies Press, 1991.
- [2] M. Lieberman and A. Lichtenberg, *Principles of Plasma Discharges and Materials Processing*. Hoboken, N.J.: Wiley-Interscience, 2005.
- [3] National Research Council, *Plasma Processing and Processing Science*. Washington, DC: The National Academies Press, 1995.
- [4] P. Gould and M. Hsing, "Design, fabrication, and characterization of a compact deep reactive ion etching system for MEMS processing," Master's thesis, Massachusetts Institute of Technology, Cambridge, MA, 2014.

- [5] I. El-Fayoumi and I. Jones, "Measurement of the induced plasma current in a planar coil, low-frequency, RF induction plasma source," *Plasma Sources Science and Technology*, vol. 6, no. 2, pp. 201–211, 1997.
- [6] Y. Han, O. Leitermann, D. A. Jackson, J. M. Rivas, and D. J. Perreault, "Resistance compression networks for radio-frequency power conversion," *IEEE Transactions on Power Electronics*, vol. 22, no. 1, pp. 41–53, Jan 2007.
- [7] N. O. Sokal, "Class-E RF power amplifiers," *QEX*, pp. 9–20, Jan/Feb 2001.
- [8] L. Roslaniec, A. S. Jurkov, A. Al Bastami, and D. J. Perreault, "Design of single-switch inverters for variable resistance/load modulation operation," *IEEE Transactions on Power Electronics*, vol. 30, no. 6, pp. 3200–3214, June 2015.
- [9] G. J. J. Winands, A. J. M. Pemen, E. J. M. van Heesch, Z. Liu, and K. Yan, "Matching a pulsed power modulator to a corona plasma reactor," in *16th IEEE International Pulsed Power Conference*, vol. 1, June 2007, pp. 587–590.
- [10] Y. Lim, H. Tang, S. Lim, and J. Park, "An adaptive impedance-matching network based on a novel capacitor matrix for wireless power transfer," *IEEE Transactions on Power Electronics*, vol. 29, no. 8, pp. 4403–4413, Aug 2014.
- [11] H. M. Nemati, C. Fager, U. Gustavsson, R. Jos, and H. Zirath, "Design of varactor-based tunable matching networks for dynamic load modulation of high power amplifiers," *IEEE Transactions on Microwave Theory and Techniques*, vol. 57, no. 5, pp. 1110–1118, May 2009.
- [12] D. Perreault, "A new architecture for high-frequency variable-load inverters," in *IEEE 17th Workshop on Control and Modeling for Power Electronics (COMPEL)*, June 2016 (in press).
- [13] A. Al Bastami, A. Jurkov, P. Gould, M. Hsing, M. Schmidt, and D. J. Perreault, "Dynamic matching system for radio-frequency plasma generation," in *2016 IEEE Energy Conversion Congress and Exposition (ECCE)*, Sept 2016, pp. 1–7.
- [14] T. W. Barton, J. M. Gordonson, and D. J. Perreault, "Transmission line resistance compression networks and applications to wireless power transfer," *IEEE Journal of Emerging and Selected Topics in Power Electronics*, vol. 3, no. 1, pp. 252–260, March 2015.
- [15] D. Perreault, J. Rivas, Y. Han, and O. Leitermann, "Methods and apparatus for resistance compression networks," May 2009, US Patent 7,535,133.
- [16] D. Perreault, "Transmission-line resistance compression networks and related techniques," September 2014, US Patent 8,830,709.
- [17] J. H. Spreen, "Electrical terminal representation of conductor loss in transformers," *IEEE Transactions on Power Electronics*, vol. 5, no. 4, pp. 424–429, Oct 1990.
- [18] E. Rotholz, "Transmission-line transformers," *IEEE Transactions on Microwave Theory and Techniques*, vol. 29, no. 4, pp. 327–331, Apr 1981.
- [19] M. Borage, K. V. Nagesh, M. S. Bhatia, and S. Tiwari, "Resonant immittance converter topologies," *IEEE Transactions on Industrial Electronics*, vol. 58, no. 3, pp. 971–978, March 2011.
- [20] P. A. Gould, M. D. Hsing, H. Q. Li, K. K. Gleason, and M. A. Schmidt, "An ultra-low cost deep reactive ion etching (drie) tool for flexible, small volume manufacturing," in *18th International Conference on Solid-State Sensors, Actuators and Microsystems*, June 2015, pp. 2268–2271.



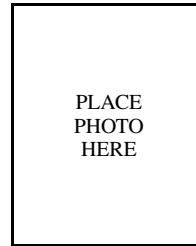
**Anas Al Bastami** (S'10) received his B.S. degree from Texas A&M University at Qatar in 2012, and his S.M. degree in 2014 from the Massachusetts Institute of Technology (MIT), both in Electrical Engineering. He is currently pursuing his Ph.D. degree in Electrical Engineering at the Laboratory for Electromagnetic and Electronic Systems (LEES) at MIT.

His interests include engineering education, and research in the areas of circuit design, embedded systems, power electronics, and renewable energy systems. Since joining MIT, he has been conducting research in various areas of interest, including radio-frequency (RF) power amplifiers and converters, impedance matching systems, and high-performance power electronic systems for a wide range of applications.

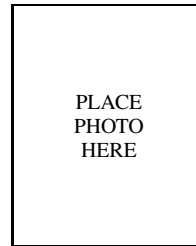


**Alexander Jurkov** (S'07) received the B.S. degree in electrical engineering and computer science from the University of Calgary, Calgary, AB, Canada in 2010, and the S.M. degree in electrical engineering from the Massachusetts Institute of Technology (MIT), Cambridge, in 2012. He is currently pursuing his Ph.D. degree in the area of power electronics and radio-frequency system design at the Laboratory for Electromagnetic and Electronic Systems at MIT.

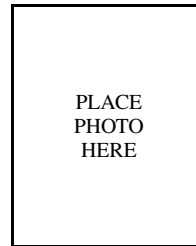
In 2012, he worked for Analog Devices Inc., Woburn, MA on the design of integrated high-speed data buffers and their realization with a 24nm technology. His research interests include RF power converters, amplifiers, combiners, and mixed-signal and embedded system design.



**Parker Gould** Biography text here.



**Mitchell Hsing** Biography text here.



**Martin Schmidt** Biography text here.



**Jung-Ik Ha** (S'97-M'01-SM'12) was born in Korea in 1971. He received the B.S., M.S., and Ph.D. degrees in electrical engineering from Seoul National University, Seoul, Korea, in 1995, 1997, and 2001, respectively.

From 2001 to 2002, he was a researcher in Yaskawa Electric Co., Japan. From 2003 to 2008, he worked for Samsung Electronics Co., Korea as a senior and principal Engineer. From 2009 to 2010, he was a chief technology officer, LS Mecapion Co., Korea. Since 2010, he has been with the department of Electrical and Computer Engineering, Seoul National University, Seoul, Korea, where he is now an associate professor. He was a visiting scholar at Massachusetts Institute of Technology from 2016 to 2017.

His research interests include power circuits and control in high efficiency and integrated electric energy conversions for various industrial fields.

PLACE  
PHOTO  
HERE

**David J. Perreault** (S'91-M'97-SM'06-F'13) received the B.S. degree from Boston University, Boston, MA, USA, and the S.M. and Ph.D. degrees from the Massachusetts Institute of Technology (MIT), Cambridge, MA. In 1997, he joined the MIT Laboratory for Electromagnetic and Electronic Systems as a Postdoctoral Associate, and became a Research Scientist in the laboratory in 1999. In 2001, he joined the MIT Department of Electrical Engineering and Computer Science, where he is currently a Professor and the Associate Department

Head. His research interests include design, manufacturing, and control techniques for power electronic systems and components, and their use in a wide range of applications. He also consults in industry, and is a Co-founder of Eta Devices, a startup company focusing on high-efficiency RF power amplifiers.

Dr. Perreault received the Richard M. Bass Outstanding Young Power Electronics Engineer Award, the R. David Middlebrook Achievement Award, the ONR Young Investigator Award, and the SAE Ralph R. Teetor Educational Award, and is a Coauthor of seven IEEE prize papers.